Modelling and Simulation in Materials Science and Engineering

PURPOSE-LED PUBLISHING™

PAPER

Modeling the structural and electronic properties of tetragonal $BaTiO_3$: a comparative study using density functional and many-body approaches

To cite this article: Newman Amoyaw *et al* 2026 *Modelling Simul. Mater. Sci. Eng.* **34** 045003

View the article online for updates and enhancements.

You may also like

- A hybrid cluster-expansion–informed machine learning framework for predicting enthalpy of mixing in BCC refractory binary alloys
Shanker Kumar and Vikas Jindal

- The co-regulation mechanism for the indentation size effect and the interface in Nb–NiTi–Nb nano-multilayer films
Dewen Yang, Bingye Huang, Xiang Chen et al.

- Multi-phase-field modelling to analyse elemental segregation during laser powder bed fusion additive manufacturing of IN625 alloy
Soma Maji, Shakti Swaroop Choudhury and Murugaiyan Amirthalingam

This content was downloaded from IP address 197.255.68.159 on 17/06/2026 at 12:45

Modelling and Simulation in Materials Science and Engineering

Check for updates

RECEIVED
17 February 2026

REVISED
24 April 2026

ACCEPTED FOR PUBLICATION
11 May 2026

PUBLISHED
20 May 2026

PAPER

Modeling the structural and electronic properties of tetragonal $BaTiO_3$: a comparative study using density functional and many-body approaches

Newman Amoyaw, Martin N Y H Egblewogbe, Samuel A Atarah and G Gebreyesus*

Department of Physics, School of Physical and Mathematical Sciences, College of Basic and Applied Sciences, University of Ghana, Accra, Ghana

* Author to whom any correspondence should be addressed.

E-mail: ghagoss@ug.edu.gh

Keywords: $BaTiO_3$, density functional theory (DFT), Hubbard U and V corrections, hybrid functionals (HSE06), G^0W^0+BSE, structural and electronic properties

Abstract

The accurate description of the structural and electronic properties of tetragonal $BaTiO_3$ remains a challenge for density functional theory (DFT) due to self-interaction errors, particularly in the partially filled Ti(3d) orbitals. In this work, we systematically investigate the performance of several first-principles approaches, including Perdew–Burke–Ernzerhof revised for solids (PBEsol), PBEsol+U, PBEsol+U+V, HSE06, and G^0W^0+Bethe–Salpeter equation (BSE), for modeling the structural and electronic properties of this prototypical ferroelectric oxide. The on-site Hubbard U (Ti(3d)) and intersite V (Ti(3d)–O(2p)) parameters are computed self-consistently using density functional perturbation theory. We show that PBEsol+U incorrectly stabilizes the cubic phase by suppressing Ti–O hybridization, whereas the inclusion of the intersite V term restores the tetragonal structure, yielding accurate lattice parameters and atomic displacements. Among the methods considered, PBEsol+U+V provides the best agreement with experimental structural data. All approaches predict an indirect band gap, with PBEsol significantly underestimating its value. Hybrid HSE06 and G^0W^0+BSE calculations yield substantially improved band gaps, with G^0W^0+BSE predicting 3.30 eV, in close agreement with experiment. While PBEsol+U+V improves the electronic structure relative to semilocal DFT, it remains less accurate than hybrid and many-body approaches. These results clarify the role of intersite interactions in stabilizing the ferroelectric phase of $BaTiO_3$ and highlight the strengths and limitations of commonly used electronic-structure methods for modeling complex oxides.

1. Introduction

Barium titanate ($BaTiO_3$, BTO) is a technologically important oxide widely exploited in electroceramics and microelectronics owing to its outstanding ferroelectric and piezoelectric properties. Its high dielectric constant combined with low dielectric losses makes it particularly suitable for a broad range of applications [1], including capacitors, multilayer ceramic capacitors, and energy-storage devices [2–8]. Moreover, doped BTO has been extensively used in positive temperature coefficient resistors and piezoelectric components, and it remains one of the most important ferroelectric ceramic materials [9, 10]. In addition to these intrinsic properties, the dielectric and structural properties of BTO are also highly sensitive to extrinsic factors such as grain size, particle size, and structural symmetry at the nanoscale [11].

BTO exhibits a sequence of temperature-driven crystallographic phase transitions, undergoing four structural transformations as a function of temperature. Above 403 K, it crystallizes in the paraelectric cubic perovskite phase with no spontaneous polarization. Upon cooling, it successively transforms into ferroelectric tetragonal (273–403 K, polarization along ($\langle 100 \rangle$)), orthorhombic (183–273 K, polarization along ($\langle 110 \rangle$)), and rhombohedral phases (below 183 K, polarization along ($\langle 111 \rangle$)) [12–16]. Among

© 2026 IOP Publishing Ltd. All rights, including for text and data mining, AI training, and similar technologies, are reserved.

these, the tetragonal phase is particularly significant because it is stable under ambient conditions and plays a central role in most device applications.

The structural, electronic, vibrational, and optical properties of BTO have been extensively investigated both experimentally and theoretically. Early first-principles studies established the microscopic origin of ferroelectricity in BTO, emphasizing the crucial role of Ti–O hybridization and lattice instabilities in driving the tetragonal distortion and spontaneous polarization [17–20]. Experimental structural investigations have provided essential benchmarks for the tetragonal phase and its lattice distortions [21], while subsequent theoretical works have examined the influence of exchange–correlation functionals and computational methodologies on the predicted structural and electronic properties [22–27]. Vibrational and dielectric properties, including phonon behavior and optical responses, have also been studied in detail both experimentally and theoretically [28, 29]. More recent investigations have explored finite-temperature effects, domain-related phenomena, and advanced polarization mechanisms using modern first-principles and multiscale approaches [30–33]. Despite these extensive efforts, accurately reproducing the tetragonal distortion and related ferroelectric properties within first-principles frameworks remains a long-standing challenge. This difficulty arises from the delicate balance between lattice distortions and Ti–O hybridization that governs ferroelectricity.

Density functional theory (DFT) [34, 35] has become a cornerstone of computational materials science, providing an efficient first-principles framework for predicting structural and electronic properties. Despite its success, the widely used local density approximation (LDA) and generalized gradient approximation (GGA) exchange–correlation functionals suffer from self-interaction errors, which are particularly pronounced in systems with localized or partially occupied *d* states [36–38]. As a prototypical ferroelectric oxide with partially occupied Ti(3*d*) states, BTO is especially sensitive to these limitations. Consequently, LDA and GGA functionals often overestimate or underestimate lattice parameters and significantly underestimate electronic properties, particularly band gaps [27, 39–41].

Recent developments in exchange–correlation functionals, such as the Strongly Constrained and Appropriately Normed (SCAN) meta-GGA functional [42, 43], have demonstrated improved predictive accuracy for both structural and electronic properties relative to LDA and GGA functionals [27]. In parallel, the Perdew–Burke–Ernzerhof revised for solids (PBEsol) functional [44], particularly when combined with the vdW-DF-C09 nonlocal correction [45], has been reported to reproduce the structural parameters of tetragonal $BaTiO_3$ with errors below 3 Despite these improvements, ferroelectric oxides remain extremely sensitive to small variations in lattice parameters and internal atomic displacements. To further mitigate self-interaction errors, numerous studies have employed DFT+*U* approaches, introducing Hubbard corrections on Ti(3*d*) and, in some cases, O(2*p*) states [26, 46–53]. However, most of these works rely on empirically chosen *U* parameters, which may limit transferability and predictive reliability. More recent investigations, particularly for the rhombohedral phase, have shown that applying a *U* correction solely to Ti(3*d*) states can induce excessive localization on Ti sites, artificially weakening Ti–O hybridization and consequently destabilizing the expected ferroelectric distortion [54].

Building on these considerations, an alternative way is the inclusion of intersite Hubbard *V* interactions within the DFT+*U*+*V* formalism, which explicitly captures the covalent nature of Ti–O bonding. Although this approach has shown promising performance in describing structural distortions and electronic properties in rhombohedral BTO, systematic investigations of the tetragonal phase employing fully first-principles, self-consistently computed *U* and *V* parameters are still lacking. This gap limits a rigorous investigation of the role of intersite Hubbard correlations in stabilizing the ferroelectric distortion at ambient conditions. In parallel, hybrid exchange–correlation functionals such as HSE06 [55] and many-body perturbation theory methods based on the GW approximation, combined with the Bethe–Salpeter equation (GW+BSE) [56–58], offer a more accurate description of quasiparticle and optical excitation energies, though at a substantially higher computational cost.

Therefore, a comprehensive and consistent comparison between semilocal functionals, first-principles DFT+*U*+*V*, hybrid functionals, and GW+BSE for tetragonal BTO is essential to (i) clarify the interplay between structural accuracy and electronic correlations, (ii) establish the reliability of first-principles Hubbard corrections for ferroelectric oxides, and (iii) provide a predictive framework for modeling their functional properties.

In this work, we present a first-principles investigation of the structural and electronic properties of tetragonal BTO using PBEsol, PBEsol+*U*, PBEsol+*U*+*V*, the hybrid HSE06 functional, and the G^0W^0+BSE approach. The on-site and intersite Hubbard parameters *U*& *V* are computed self-consistently within density-functional perturbation theory (DFPT) using a linear-response formalism [59–62]. We demonstrate that applying the on-site Hubbard *U* correction alone drives the tetragonal

BTO toward a cubic configuration by suppressing Ti–O hybridization, whereas the inclusion of intersite Hubbard V correction restores covalency and stabilizes the tetragonal distortion. The optimized lattice parameters and atomic distortions obtained with PBEsol+U+V shows significantly improved agreement with experimental lattice parameters and atomic displacements compared to other semilocal functionals. Analysis of the electronic structure reveals that the projected density of states (PDOS) remains qualitatively similar across methods, while band gaps are strongly method dependent. In particular, G^0W^0+BSE produces band gaps in excellent agreement with experiment, whereas semilocal functionals consistently underestimate the gap. These findings provide a comprehensive picture of the interplay between structural distortions, Ti–O hybridization, and electronic properties in tetragonal BTO, highlighting the critical role of first-principles intersite Hubbard corrections and advanced electronic-structure methods in accurately modeling ferroelectric oxides.

The remainder of this paper is organized as follows: section II presents the computational details, section III presents the analysis of the structural and electronic results, and section IV summarizes the main conclusions.

2. Computational details

The first-principles calculations were performed using the plane-wave pseudopotential method as implemented in Quantum ESPRESSO [63, 64]. The generalized GGA with PBEsol parameterization [44] was employed for the semi-local and Hubbard-corrected DFT calculations, along with ultrasoft pseudopotentials (USPP) [65], which provide an optimal balance between computational efficiency and accuracy for structural and electronic properties. The pseudopotentials used were for Ba: Ba.pbesol-spn-rrkjus_psl.1.0.0.UPF, Ti:Ti.pbesol-spn-rrkjus_psl.1.0.0.UPF, and O:O.pbesol-n-rrkjus_psl.1.0.0.UPF. The use of the same USPP set for PBEsol, PBEsol+U, and PBEsol+U+V ensures that differences in these results arise primarily from the exchange-correlation treatment and Hubbard corrections rather than from the underlying ionic potentials.

Convergence tests with respect to plane-wave cutoff energy and **k**-point sampling were performed for all computational methods considered. The selected parameters ensure total-energy convergence within approximately 1 meV atom^{-1}. These parameters were further verified to yield converged structural and electronic properties across all exchange-correlation treatments considered. To enable a consistent comparison within each methodological methods, the same cutoff energies and **k**-point grids were adopted throughout. A kinetic-energy cutoff of 80 Ry was used for the wave functions, and 800 Ry for the charge density. Brillouin-zone integrations were carried out using **k**-point meshes of $12 \times 12 \times 12$ for ground-state calculations and $18 \times 18 \times 18$ for PDOS calculations.

The on-site U and intersite V Hubbard parameters were computed self-consistently using DFPT [60, 62] as implemented in the HP code [66] of Quantum ESPRESSO [63, 64]. Löwdin-orthogonalized atomic orbitals were employed as Hubbard projector functions [61]. To ensure accuracy, the convergence of U and V with respect to **k** and **q** meshes was systematically evaluated. As shown in figure 1, optimal meshes were determined to be $6 \times 6 \times 6$ for **k** points and $4 \times 4 \times 4$ for **q** points.

Using these meshes, the Hubbard parameters were computed iteratively through a self-consistent cycle of structural optimizations and recalculation of U and V for each updated geometry, until convergence was achieved for both the structure and the Hubbard parameters, with accuracies of approximately 0.01 eV for U and 0.001 eV for V. The final self-consistent parameters were $U = 4.52$ eV for Ti(3d) within PBEsol+U and $U = 5.21$ eV for Ti(3d) with intersite V values ranging from 1.17 eV to 1.37 eV in PBEsol+U+V, depending on the Ti–O distance. These values are consistent with previous reports [54], though the structural and electronic properties of tetragonal BTO were not addressed in that work. The optimized structural parameters obtained using PBEsol, PBEsol+U, and PBEsol+U+V are listed in table 1 and were subsequently used for electronic structure calculations.

Hybrid functional calculations were performed using HSE06 [55] with optimized norm-conserving Vanderbilt pseudopotentials [67] and a mixing parameter of 25%.

For G^0W^0 calculations, the all-electron exciting code [68] was employed. **k**-point meshes of $4 \times 4 \times 4$ and **q**-point meshes of $6 \times 6 \times 6$ were used. Electronic properties were computed within the G^0W^0 approximation using the PBEsol-optimized structures, and the BSE was subsequently solved to obtain the optical spectrum and accurate band gap energies.

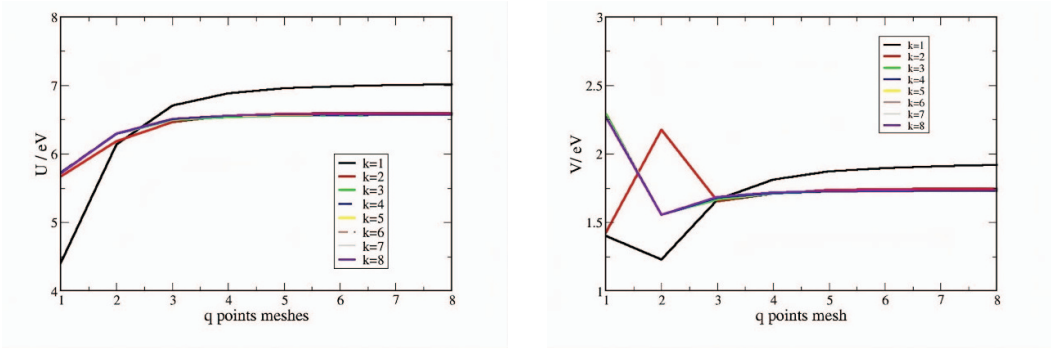

(a) Convergence of onsite U with respect to **k** and **q** meshes.

(b) Convergence of intersite V with respect to **k** and **q** meshes

Figure 1. Convergence of the onsite U and intersite V Hubbard parameters with respect to **k** and **q** meshes within PBEsol+U+V.

3. Results and discussion

3.1. Structural parameters

In this subsection, we present and discuss the results of structural optimizations for tetragonal BTO with space group P4mm (No. 99) [12, 69] using various functionals and methods. The tetragonal structure is characterized by lattice parameters a and c, atomic displacements, unit cell volume, and the c/a ratio. Our results, together with previous DFT-based theoretical data [23, 27] and experimental measurements [12, 69], are summarized in table 1.

Previous studies using the PBEsol functional [27] reported slight overestimations of a (0.23%) and c (4.33%), as well as the c/a ratio (4.08%) and unit cell volume (4.90%). In contrast, LDA typically underestimates cell parameters [23, 24], while PBE [70] and PBE0 [23] tend to perform poorly in predicting tetragonal BTO structure. Our results show that among the tested functionals, PBEsol+U+V provides the most accurate structural predictions, whereas PBEsol+U performs the worst. This is consistent with previous studies on rhombohedral BTO [54], where PBEsol+U+V demonstrated superior accuracy in reproducing experimental lattice parameters and distortions. Notably, PBEsol+U incorrectly stabilizes a cubic ground-state configuration, deviating from the tetragonal phase, consistent with previous studies for the rhombohedral BTO [54]. This discrepancy arises from PBEsol+Uś oversimplification of electron correlations, localizing only the Ti(3d) electron and neglecting the crucial hybridization between Ti(3d) and O(2p) orbitals.

The poor performance of PBEsol+U arises from its incomplete treatment of electron interactions. In contrast, PBEsol+U+V incorporates intersite Hubbard interactions V, which explicitly account for Ti(3d)–O(2p) hybridization. This more complete description of the electronic structure enables more accurate predictions of lattice parameters, atomic displacements, and the correct tetragonal phase. Quantitatively, PBEsol+U+V deviates from experimental values by 0.48% for a, 1.16% for c, 1.64% for c/a, and 0.23% for unit cell volume, whereas PBEsol alone yields slightly better agreement for c (0.30%) and c/a ratio (0.96%), consistent with previous reports [30]. Importantly, PBEsol+U+V also predicts atomic displacements more accurately than PBEsol, SCAN, HSE06, and LDA functionals as shown in table 1.

Hybrid HSE06 calculations yield comparatively poorer structural predictions, ranking second worst after PBEsol+U. This behavior aligns with prior studies indicating that hybrid functionals, optimized primarily for band-gap accuracy, do not necessarily improve equilibrium geometries [27]. In ferroelectric oxides such as BTO, structural parameters including lattice constants, atomic displacements, and Ti–O hybridization critically influence electronic structure and polarization properties. Therefore, an accurate and self-consistent description of the tetragonal structure is essential for reliable prediction of both electronic and ferroelectric behavior, highlighting the importance of employing functionals that balance structural and electronic accuracy.

Table 1. Optimized lattice parameters, atomic displacements, unit-cell volume, and tetragonality (c/a) of BTO obtained using PBEsol, PBEsol+U+V, HSE06, and PBEsol+U, compared with previous DFT results [27] and experimental data [12, 69]. Atomic displacements are defined relative to the cubic reference structure of BTO.

Functional	a (Å)	c (Å)	c/a	V (Å^3)	δ(Ti) (Å)	$\delta(O_1)$ (Å)	$\delta(O_2)$ (Å)
PBEsol	3.964	4.053	1.0224	63.69	0.015	–0.030	–0.019
PBEsol+U+V	3.972	4.088	1.0293	64.50	0.016	–0.035	–0.022
HSE06	4.025	4.259	1.0581	69.00	0.0252	–0.0216	–0.0627
LDA [23]	3.952	3.987	1.0089	—	0.0115	–0.0168	–0.0107
PBE [70]	3.976	4.172	1.0493	67.50	0.0188	–0.0473	–0.0266
PBEsol [27]	4.000	4.216	1.0540	67.50	0.018	—	—
SCAN [27]	3.985	4.101	1.0290	65.10	0.017	—	—
HSE06 [27]	3.959	4.113	1.0390	64.50	0.019	—	—
PBE0 [23]	3.968	4.137	1.0426	—	0.0203	–0.0431	–0.0226
* PBEsol+U	3.990	3.990	1.0000	63.52	0.000	0.000	0.000
Experiment	3.991 [69]	4.041 [69]	1.0127 [69]	64.35 [69]	0.024 [69]	–0.043 [69]	–0.033 [69]

*PBEsol+U predicts a cubic ground-state geometry.

3.2. Electronic properties

In this subsection, we first present and discuss the computed projected density of states (PDOS) of tetragonal BTO obtained using PBEsol, PBEsol+U, PBEsol+U+V, and HSE06. Subsequently, the band structures and band gaps calculated with PBEsol, PBEsol+U+V, HSE06, G^0W^0, and G^0W^0+BSE are analyzed and compared with available theoretical and experimental data.

The total and PDOS calculated with the different functionals are shown in figure 2. The PDOS indicates that the valence-band maximum is dominated by O(2p) states, with smaller contributions from Ti(3d) orbitals, whereas the conduction-band minimum is primarily composed of Ti(3d) states with minor O(2p) contributions. This distribution is consistent with previous theoretical studies of tetragonal BTO [24, 30, 71]. The Ti–O hybridization, reflecting the covalent character of bonding, plays a crucial role in stabilizing the ferroelectric phase and is highly sensitive to Hubbard corrections, as discussed in section 3.1 and in [54] for rhombohedral BTO.

Introducing Hubbard interactions produces moderate modifications in the PDOS, mainly reflected in shifts of the conduction-band states and slight changes in spectral weight, as shown in figure 2(a). While the overall orbital character remains qualitatively similar across all functionals, PBEsol+U shows noticeable changes compared with PBEsol and PBEsol+U+V, indicating the impact of on-site and intersite corrections on Ti–O hybridization. A noticeable upward shift of the conduction-band energies is observed for PBEsol+U+V and HSE06 relative to PBEsol, in agreement with earlier findings for rhombohedral BTO [54].

The consistent orbital contributions, together with functional-dependent conduction-band shifts, provide insight into the electronic structure of tetragonal BTO and highlight the sensitivity of predicted electronic properties to the treatment of exchange–correlation effects.

Overall, comparison of PDOS results demonstrates that hybrid HSE06 provides an improved description of conduction-band energies, while PBEsol+U+V offers a balanced representation that captures both hybridization effects and band-edge shifts, bridging the gap between semilocal and many-body approaches.

The band structures computed using PBEsol, PBEsol+U+V, HSE06, and G^0W^0 are shown in figure 3. For the 5-atom unit cell of $BaTiO_3$, semi-local DFT calculations scale as $\mathcal{O}(N^3)$ and remain computationally inexpensive. The inclusion of Hubbard U and intersite V terms introduces only a modest overhead (typically less than a factor of 2). In contrast, HSE06 calculations are approximately one to two orders of magnitude more expensive due to the evaluation of nonlocal exchange, while G_0W_0 and G_0W_0+BSE calculations further increase the computational cost by up to two orders of magnitude. This highlights the efficiency of the PBEsol+U+V approach in capturing key physical effects at significantly reduced computational cost.

All approaches predict an indirect band gap, with the valence-band maximum located at the A point and the conduction-band minimum at the Γ point, in agreement with previous theoretical studies [41, 54, 70, 72, 73].

As expected, the semi-local PBEsol functional significantly underestimates the band gap. The inclusion of on-site and intersite Hubbard corrections in PBEsol+U+V leads to a substantial improvement,

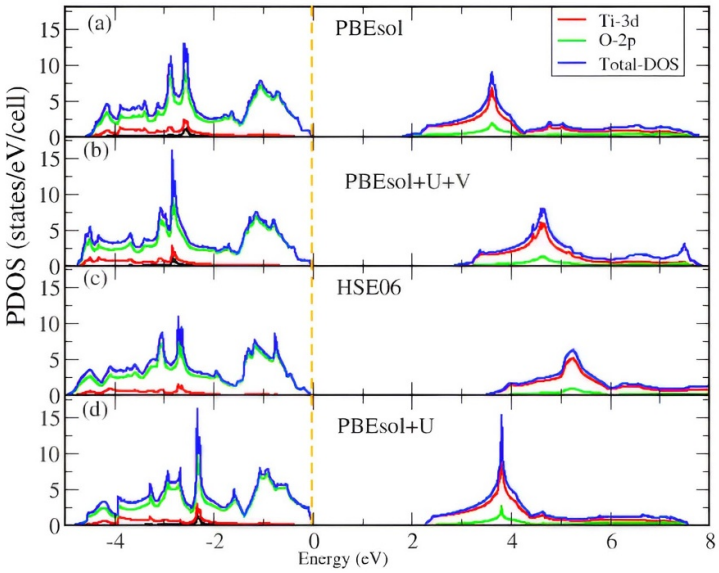

Figure 2. Total and projected density of states of tetragonal BTO computed using (a) PBEsol, (b) PBEsol+U+V, (c) HSE06, and (d) PBEsol+U (for which the optimized structure is cubic). The energy axis is referenced to the valence-band maximum of each method.

reducing the discrepancy with experiment to approximately 16%, in agreement with previous findings that emphasize the role of Ti(3d)–O(2p) hybridization in determining the electronic structure [24, 30, 54, 71].

The hybrid HSE06 functional provides a highly accurate estimate of the band gap, with a deviation of less than 3% from experimental values [74]. In contrast, the G^0W^0 quasiparticle correction yields a band gap of 3.73 eV, corresponding to an overestimation of about 10%. This behavior reflects the quasiparticle nature of the G^0W^0 approximation, while electron–hole interactions, included only at the BSE level, are essential for accurately describing optical excitations.

The inclusion of excitonic effects through the BSE leads to a reduction of the optical gap, bringing the theoretical prediction into closer agreement with experimental value. From the difference between the quasiparticle gap obtained within G^0W^0 and the onset of the BSE absorption spectrum, the exciton binding energy is estimated to be approximately 0.4 eV, highlighting the importance of electron–hole interactions in $BaTiO_3$. Furthermore, the computed imaginary part of the dielectric function, $\epsilon(\omega)$, shown in figure 4, reveals that excitonic effects significantly enhance the absorption onset and modify the spectral features near the band edge compared to the independent-particle picture.

The indirect band gap along the A–Γ pathway plays an important role in determining the optical response of tetragonal BTO, influencing both light absorption and the coupling between electronic and ferroelectric properties.

Furthermore, the electronic structure is strongly coupled to lattice dynamics. The accurate description of Ti(3d)–O(2p) hybridization, improved within the PBEsol+U+V framework, plays a key role in stabilizing the ferroelectric distortion and is directly linked to the soft phonon modes responsible for the tetragonal phase. In this sense, the improved band gap and electronic structure are consistent with a more realistic description of the underlying lattice instabilities.

Table 2 summarizes the computed band gaps for tetragonal BTO in comparison with previous theoretical and experimental results. The PBEsol value underestimates the gap by roughly 47%, consistent with earlier reports [27, 30]. Among the considered approaches, the most accurate agreement with experiment is achieved when many-body corrections are included, particularly through G^0W^0 combined with BSE analysis, which accounts for excitonic effects beyond standard DFT. The excitonic binding energy is estimated to be approximately 0.4 eV.

Overall, these results provide a comprehensive picture of the electronic structure of tetragonal BTO and underscore the importance of advanced exchange correlation treatments for quantitatively reliable predictions of band gaps and optical properties.

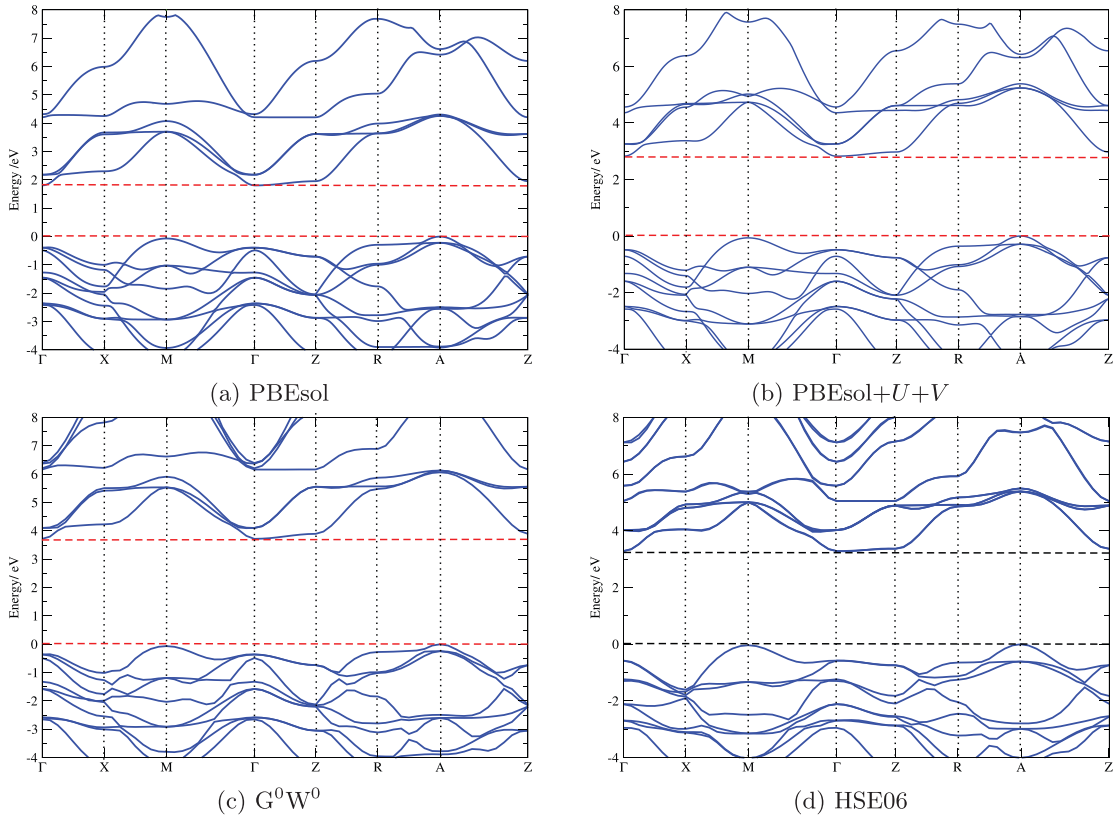

Figure 3. Electronic band structures of tetragonal BTO computed using (a) PBEsol, (b) PBEsol+U+V, (c) G^0W^0, and (d) HSE06. The energy axis is referenced to the valence-band maximum of each method.

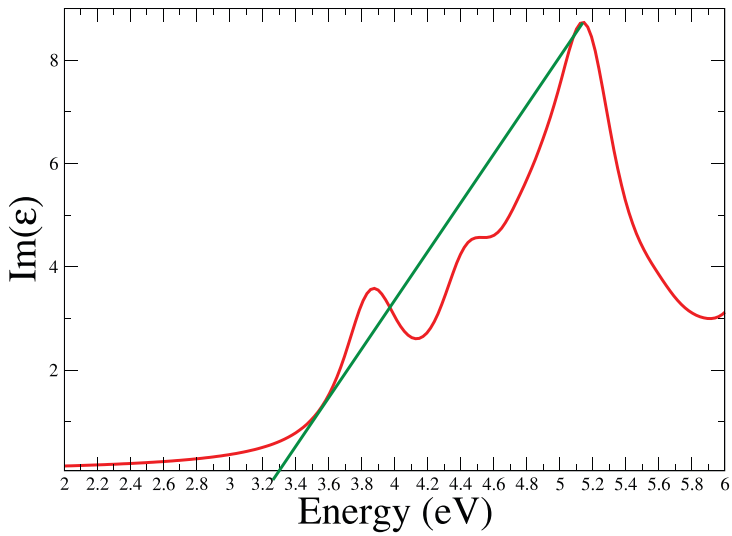

Figure 4. Im[$\epsilon(\omega)$] of tetragonal BaTiO computed within the G^0W^0+BSE method. The inclusion of electron–hole interactions enhances the absorption onset and modifies the spectral features near the band edge, highlighting the importance of excitonic effects in the optical response.

Table 2. Computed band gaps of tetragonal BTO obtained using PBEsol, PBEsol+U+V, HSE06, G^0W^0, and G^0W^0+BSE, with comparison to previous DFT results [27] and experimental values [74]. The PBEsol+U optimization yields a cubic structure; therefore, the corresponding band gap is reported for cubic BTO.

Functional	Band gap (E_g) (eV)
PBEsol	1.80
PBEsol+U+V	2.83
HSE06	3.28
LDA [27]	1.72
PBE [70]	1.6
PBEsol [27]	1.73
SCAN [27]	2.13
HSE06 [27]	3.27
PBE0 [23]	4.1
G^0W^0	3.73
G^0W^0+BSE	3.30
* PBEsol+U	2.27
Experiment	3.38 [74]

4. Conclusion

We performed a comparative first-principles study of tetragonal BTO to assess the performance of several exchange-correlation approaches in describing its structural, electronic, and optical properties. The results show that PBEsol+U+V provides the most accurate structural description, correctly stabilizing the tetragonal phase and reproducing lattice parameters and ferroelectric distortions. In contrast, PBEsol+U alone incorrectly favors a cubic structure, demonstrating that intersite interactions are essential to capture Ti–O hybridization.

All methods predict an indirect band gap along A–Γ, but the gap magnitude is strongly functional-dependent. PBEsol significantly underestimates the gap, while PBEsol+U+V partially corrects it. HSE06 yields a band gap in close agreement with experiment, while G^0W^0 overestimates the quasiparticle gap. The inclusion of excitonic effects through the BSE reduces the optical gap and improves agreement with the experimental value, with an estimated exciton binding energy of approximately 0.4 eV.

PDOS analysis indicates a valence band dominated by O(2p) states and a Ti(3d)-dominated conduction band, with the degree of Ti-O hybridization highly sensitive to correlation effects. This improved electronic description is consistent with the stabilization of the ferroelectric distortion and the underlying lattice instabilities.

Overall, the study demonstrates that PBEsol+U+V offers the best balance between structural accuracy and computational cost, whereas hybrid and many-body methods remain necessary for quantitatively reliable band gaps and optical spectra. These findings provide practical guidance for modeling ferroelectric oxides and related functional materials.

Acknowledgments

The authors gratefully acknowledge insightful collaborations with Lorenzo Bastonero, Michele Kotiuga, Iurii Timrov, and Nicola Marzari on the rhombohedral phase of $BaTiO_3$, reported in Physical Review B 108, 235171 (2023), which provided important conceptual and methodological groundwork for the present study. The authors also acknowledge support from the Abdus Salam International Centre for Theoretical Physics (ICTP). Computational resources were provided by the Centre for High Performance Computing (CHPC), South Africa.

Data availability statement

The data that support the findings of this study are available upon reasonable request from the authors.

Author contributions

Newman Amoyaw 0009-0009-5785-6890
Data curation (equal), Formal analysis (equal), Investigation (equal), Methodology (equal), Writing – original draft (equal)

Martin N Y H Egblewogbe 0000-0001-5921-4300
Data curation (equal), Formal analysis (equal), Investigation (equal), Supervision (equal), Writing – review & editing (equal)

Samuel A Atarah 0000-0003-2479-0556
Formal analysis (equal), Writing – original draft (equal), Writing – review & editing (equal)

G Gebreyesus 0000-0002-3413-2349
Conceptualization (lead), Data curation (equal), Formal analysis (equal), Investigation (lead), Methodology (equal), Resources (equal), Supervision (lead), Validation (equal), Writing – original draft (equal), Writing – review & editing (lead)

References

[1] Baraskar B G, Kadhane P S, Darvade T C, James A R and Kambale R C 2018 Batio3-based lead-free electroceramics with their ferroelectric and piezoelectric properties tuned by ca2+, sn4+ and zr4+ substitution useful for electrostrictive device application *Ferroelectrics and Their Applications* ed H Irzaman (IntechOpen)
[2] Peng W *et al* 2020 *Adv. Funct. Mater.* **30** 1910569
[3] Rubio-Marcos F, Ochoa D A, Del Campo A, García M A, Castro G R, Fernández J F and García J E 2018 *Nat. Photon.* **12** 29–32
[4] Sanna S, Thierfelder C, Wippermann S, Sinha T P and Schmidt W G 2011 *Phys. Rev. B* **83** 054112
[5] Waser R 2003 *Nanoelectronics and Information Technology: Advanced Electronic Materials and Novel Devices* 3rd edn (Wiley-VCH)
[6] De U, Sahu K R and De A 2015 *Solid State Phenom.* **232** 235–78
[7] Mahadeva S K, Walus K and Stoeber B 2015 Piezoelectric paper for physical sensing applications *28th IEEE Int. Conf. on Micro Electro Mechanical Systems (MEMS)* p 861
[8] Vasta G, Jackson T J and Tarte E 2012 *Thin Solid Films* **520** 3071–8
[9] Belgrade S 2008 History and challenges of barium titanate: Part II (available at: https://api.semanticscholar.org/CorpusID:138681088)
[10] Tihtih M, Ibrahim J E F M, Basyooni M A, En-nadir R, Belaid W, Hussainova I and Kocserha I 2023 *ACS Omega* **8** 8448–60
[11] Tihtih M, Basyooni-M Kabatas M A, En-nadir R and Kocserha I 2026 *Nanomaterials* **16** 96
[12] Kwei G H, Lawson A C, Billinge S J L and Cheong S W 1993 *J. Phys. Chem.* **97** 2368–77
[13] Kay H F 1948 *Acta Crystallogr.* **1** 229–37
[14] Merz W J 1949 *Phys. Rev.* **76** 1221–5
[15] Devonshire A 1954 *Adv. Phys.* **3** 85–130
[16] Park S E, Wada S, Cross L E and Shrout T R 1999 *J. Appl. Phys.* **86** 2746–50
[17] Cohen R E and Krakauer H 1990 *Phys. Rev. B* **42** 6416
[18] King-Smith R and Vanderbilt D 1992 *Ferroelectrics* **136** 85–94
[19] Ghosez P, Gonze X, Lambin P and Michenaud J P 1995 *Phys. Rev. B* **51** 6765(R)
[20] Ghosez P, Gonze X and Michenaud J P 1999 *Ferroelectrics* **220** 1
[21] Hewat A W 1973 *Ferroelectrics* **6** 215–8
[22] Wang J J, Wu P P, Ma X Q and Chen L Q 2010 *J. Appl. Phys.* **108** 114105
[23] Evarestov R A and Bandura A V 2012 *J. Comput. Chem.* **33** 1123
[24] Goh E, Ong L, Yoon T and Chew K 2016 *Comput. Mater. Sci.* **117** 306
[25] Mahmoud A, Erba A, El-Kelany K E, Rérat M and Orlando R 2014 *Phys. Rev. B* **89** 045103
[26] Tsunoda N, Kumagai Y and Oba F 2019 *Phys. Rev. Mater.* **3** 114602
[27] Zhang Y, Sun J, Perdew J P and Wu X 2017 *Phys. Rev. B* **96** 035143
[28] Hermet P, Veithen M and Ghosez P 2009 *J. Phys.: Condens. Matter* **21** 215901
[29] Seo Y S and Ahn J S 2013 *Phys. Rev. B* **88** 014114
[30] Mellaerts S, Seo J W, Afanas'ev V, Houssa M and Locquet J P 2022 *Phys. Rev. Mater.* **6** 064410
[31] Yuk S F, Pitike K C, Nakhmanson S M, Eisenbach M, Li Y W and Cooper V R 2017 *Sci. Rep.* **7** 43482
[32] Royo M, Hahn K R and Stengel M 2020 *Phys. Rev. Lett.* **125** 217602
[33] Kotiuga M, Halilov S, Kozinsky B, Fornari M, Marzari N and Pizzi G 2022 *Phys. Rev. Res.* **4** L012042
[34] Hohenberg P and Kohn W 1964 *Phys. Rev.* **136** B864
[35] Kohn W and Sham L 1965 *Phys. Rev.* **140** A1133
[36] Kulik H, Cococcioni M, Scherlis D and Marzari N 2006 *Phys. Rev. Lett.* **97** 103001
[37] Kulik H and Marzari N 2008 *J. Chem. Phys.* **129** 134314
[38] Cohen A, Mori-Sánchez P and Yang W 2008 *Science* **321** 792
[39] Lopez-Candales G, Tang Z, Xia W, Jia F and Zhang P 2021 *Phys. Rev. B* **103** 035128
[40] Zhang H Y Zeng Z Y Zhao Y Q, Lu Q Cheng Y 2016 *Z. Naturforsch. A* **71** 759–68
[41] Mohammed Tihtih Jamal Eldin F M Ibrahim M A B W B L A G and Kocserha I 2022 *Mater. Technol.* **37** 2995–3005
[42] Sun J *et al* 2016 *Nat. Chem.* **8** 831–6
[43] Sun J, Ruzsinszky A and Perdew J P 2015 *Phys. Rev. Lett.* **115** 036402
[44] Perdew J P, Ruzsinszky A, Csonka G I, Vydrov O A, Scuseria G E, Constantin L A, Zhou X and Burke K 2008 *Phys. Rev. Lett.* **100** 136406

[45] Cooper V R 2010 *Phys. Rev. B* **81** 161104
[46] Zhang J, Gou G and Pan B 2014 *J. Phys. Chem. C* **118** 17254
[47] Erhart P, Klein A, Aberg D and Sadigh B 2014 *Phys. Rev. B* **90** 035204
[48] Liu X, Bjorheim T S and Haugsrud R 2017 *J. Mater. Chem. A* **5** 1050
[49] Chen H and Millis A 2017 *Sci. Rep.* **7** 6142
[50] Watanabe Y 2018 *J. Chem. Phys.* **148** 194702
[51] Majumder S, Basera P, Tripathi M, Choudhary R, Bhattacharya S, Bapna K and Phase D 2019 *J. Phys.: Condens. Matter* **31** 205001
[52] Din N, Jiang T, Gholam-Mirzaei S, Chini M and Turkowski V 2020 *J. Phys.: Condens. Matter* **32** 475601
[53] Dwij V, De B, Sharma G, Shukla D, Gupta M, Mittal R and Sathe V 2022 *Physica B* **624** 413381
[54] Gebreyesus G, Bastonero L, Kotiuga M, Marzari N and Timrov I 2023 *Phys. Rev. B* **108** 235171
[55] Heyd J, Scuseria G E and Ernzerhof M 2003 *J. Chem. Phys.* **118** 8207–15
[56] Hedin L 1965 *Phys. Rev.* **139** A796–823
[57] Godby R W, Schlüter M and Sham L J 1988 *Phys. Rev. B* **37** 10159–75
[58] Hybertsen M S and Louie S G 1986 *Phys. Rev. B* **34** 5390–413
[59] Cococcioni M and de Gironcoli S 2005 *Phys. Rev. B* **71** 035105
[60] Timrov I, Marzari N and Cococcioni M 2018 *Phys. Rev. B* **98** 085127
[61] Timrov I, Aquilante F, Binci L, Cococcioni M and Marzari N 2020 *Phys. Rev. B* **102** 235159
[62] Timrov I, Marzari N and Cococcioni M 2021 *Phys. Rev. B* **103** 045141
[63] Giannozzi P *et al* 2009 *J. Phys.: Condens. Matter* **21** 395502
[64] Giannozzi P *et al* 2017 *J. Phys.: Condens. Matter* **29** 465901
[65] Dal Corso A 2014 *Comput. Mater. Sci.* **95** 337–50
[66] Timrov I, Marzari N and Cococcioni M 2022 *Comput. Phys. Commun.* **278** 108455
[67] Hamann D R 2013 *Phys. Rev. B* **88** 085117
[68] Gulans A, Kontur S, Meisenbichler C, Nabok D, Pavone P, Rigamonti S, Sagmeister S, Werner U and Draxl C 2014 *J. Phys.: Condens. Matter* **26** 363202
[69] Yasuda N *et al* 2009 *J. Synchrotron Radiat.* **16** 352–7
[70] Uludogan M, Guarin D P, Gomez Z E, Cagin T and Goddard W 2008 *Comput. Model. Eng. Sci.* **24** 215
[71] Cohen R E and Krakauer H 1992 *Ferroelectrics* **136** 65–83
[72] Salehi H, Shahtahmasebi N and Hosseini S M 2003 *Eur. Phys. J. B* **32** 177–80
[73] Razak N A A, Zabidi N A and Rosli A N 2017 *AIP Conf. Proc.* **1875** 020017
[74] Wemple S H 1970 *Phys. Rev. B* **2** 2679–89